Available online at www.sciencedirect.com
ScienceDirect
Trans. Nonferrous Met. Soc. China 26(2016) 1126−1137
Transactions of Nonferrous Metals Society of China
www.tnmsc.cn

Influence of sodium silicate on manganese electrodeposition in sulfate solution

Jian-rong XUE[1,2], Hong ZHONG[1], Shuai WANG[1], Chang-xin LI[1], Fang-fang WU[1]

1. School of Chemistry and Chemical Engineering, Central South University, Changsha 410083, China;
2. College of Chemistry and Chemical Engineering,
Hunan University of Science and Technology, Xiangtan 411201, China

Received 9 June 2015; accepted 6 January 2016

Abstract: The influences of sodium silicate on manganese electrodeposition in sulfate solution were investigated. Manganese electrodeposition experiments indicate that a certain amount of sodium silicate can improve cathode current efficiency and initial pH 7.0−8.0 is the optimized pH for high cathode current efficiency. The analyses of scanning electron microscopy (SEM) and X-ray diffraction (XRD) indicate the compact morphology and nanocrystalline structure of electrodeposits. X-ray photoelectron spectrometry (XPS) analysis shows that the elements of Mn, Si and O exist in the deposit. The solution chemistry calculations of sulfate electrolyte and sodium silicate solution indicate that species of Mn^{2+}, $MnSO_4$, $Mn(SO_4)_2^{2-}$, Mn^{2+}, $MnSiO_3$, $Mn(NH_3)^{2+}$, SiO_3^{2-} and $HSiO_3^-$ are the main active species during the process of manganese electrodeposition. The reaction trend between Mn^{2+} and Si-containing ions is confirmed by the thermodynamic analysis. In addition, polarization curve tests confirm that sodium silicate can increase the overpotential of hydrogen evolution reaction, and then indirectly improve the cathode current efficiency.
Key words: electrodeposition; manganese; sodium silicate; electrodeposit structure; hydrogen evolution reaction

1 Introduction

Manganese metal has been widely used in stainless steels and alloying with Ni, Zn and Sn [1−3]. Manganese is also the most electro-negative metal [4]. Metallic manganese is primarily electrodeposited from aqueous sulfate solutions. The electrolyte is composed of manganese sulfate and ammonium sulfate with trace Se-containing additive. Manganese sulfate is commonly obtained from leaching solution of manganese ores.

The rapid development of manganese industry has led to the decrease of manganese ore grade markedly. The conventional techniques used for ore beneficiation contain gravity separation, magnetic separation, froth flotation, pyrometallurgy and hydrometallurgy. The froth flotation, used as a selective processing method, is promising for ore beneficiation, as it has various advantages in terms of applicability, adaptability, operation, efficiency and economics. Sodium silicate, as depressant or dispersant, is widely used as regulating reagent in the flotation of minerals [5,6]. In iron ore flotation, sodium silicate is used to disperse the kaolinite in a wide range of pH value [7]. Regarding the flotation mechanism of sodium silicate, there are few publications available. The depression mechanism of sodium silicate is primarily the adsorption action of the hydrolysis products of sodium silicate, which produces a number of monomeric, polymeric and colloidal species. GONG et al [8] advocated that polymeric silicate species in concentrated solutions provided a depressing effect on iron oxide due to the strong adsorption of the polymeric silicate species onto the iron oxide surface, thus hindering it from collector adsorption. Sodium silicate was also widely used in the froth flotation of manganese minerals. PARRENT [9] found that the degree of selectivity of pyrolusite was fixed as sodium silicate was added in flotation of manganese oxide ores, regardless of dosages and particle sizes of sodium oleate and sodium silicate. In the study of ANDRADE et al [10], it was found that the inhibition effect of sodium silicate at pH 9.0 was more efficient in depressing quartz than rhodonite, especially for lower concentrations of sodium silica, whereas the flotation response of rhodochrosite was only slightly influenced at both pH 9.0 and pH 11.0.

Foundation item: Project (2015BAB17B01) supported by the National Science and Technology Support Program of China; Project (21376273) supported by the National Natural Science Foundation of China
Corresponding author: Hong ZHONG; Tel: +86-731-88830654; E-mail: zhongh@csu.edu.cn;
DOI: 10.1016/S1003-6326(16)64211-5

However, the adsorption of sodium silicate on manganese ore surface results in a certain amount of silicate species remaining in the floated manganese ores. These residual species at a certain level can exert some effects on the subsequent process of manganese electrodeposition.

However, manganese electrodeposition process is particularly sensitive to impurities, which significantly influence the current efficiency, morphology and crystal structure of electrodeposited manganese. This is attributed to that standard reduction potential for Mn^{2+}/Mn is −1.18 V (vs SHE). Metallic impurities can decrease the overpotential of hydrogen evolution and hence lead to the decrease of cathode current efficiency [11,12]. And the deleterious influences of metallic impurities on the morphology of zinc electrodeposit have been analyzed [13]. Thus, the impurities in the electrolyte are strictly removed to gain high purity manganese during industrial production process of metallic manganese [14]. Furthermore, appropriate additives, such as SeO_2 and SO_2, should be added into electrolyte to improve cathode current efficiency and quality of electrodeposited manganese. However, few literatures are available regarding effects of organic impurities on manganese electrodeposition process. DING et al [15] confirmed the beneficial effects of N-based auxiliary additives on manganese electrodeposition. PADHY et al [12] found that quaternary amine additives improved the morphology and crystal structure of manganese electrodeposits. As for the influence of sodium silicate on electrodeposited metal, previous study [16] indicated that the addition of silicates into the electrolyte of zinc led to the formation of a physical barrier to hinder aggressive ions from penetrating. In addition, it was reported that metal coatings can be electrodeposited from Si-containing electrolyte to improve the morphology and anti-corrosion behavior [17,18]. However, information regarding the effect of silicate species on manganese electrodeposition is not available.

In this work, the influences of sodium silicate on manganese electrodeposition were investigated systematically, based on the analyses of manganese electrodeposition experiments, characterization of scanning electron microscopy (SEM), energy dispersive spectroscopy (EDS), X-ray diffraction (XRD) pattern, X-ray photoelectron spectrometry (XPS) analysis, solution chemistry calculations, thermodynamics and cathode polarization.

2 Experimental

2.1 Reagents and solutions

The catholyte contained analytical grade manganese sulfate, ammonium sulfate, selenium dioxide and sodium silicate. Ammonia and sulfuric acid were used to adjust the pH of the catholyte. Reagents of analytical grade are dissolved in deionized water. Unless otherwise specified, catholyte components were as follows: 0.55 mol/L Mn^{2+}, 0.91 mol/L $(NH_4)_2SO_4$, 3.6×10^{-4} mol/L SeO_2, 8.2×10^{-4} mol/L Na_2SiO_3 and pH 7.0. The anolyte contained 0.91 mol/L $(NH_4)_2SO_4$.

2.2 Electrodeposition experiment

The experiments of electrodepositing manganese were carried out in a divided plexiglass cell, which consisted of anode and cathode compartments (each effective volume of 100 mL) separated by a diaphragm, a cathode and an anode. The cathode was used with AISI 301 stainless steel sheet and polished with metallographic sandpaper, with a geometrical surface area of 27 mm×70 mm (single-side effective surface area of 1080 mm^2), and a thin layer of epoxy resin was coated on the other surface. The cathode was rinsed with acetone and deionized water. Prior to electrodeposition experiment, the cathode was immersed in a 4% Na_2SiO_3 solution for 5 min. $PbSn_{0.4}Ag_{0.014}Sb_{0.014}$ alloy was used as anode with a geometrical surface area of 20 mm× 70 mm (single-side effective surface area of 740 mm^2), and a thin layer of epoxy resin was also applied on the other surface. The anode and cathode were placed at a constant distance of 12.0 mm from the diaphragm. The electrolyte temperature was controlled within (30±1) °C by a thermostatic control. The catholyte was mixed by magnetic stirring. The experiments of electrodepositing manganese were carried out subsequently. After electrolysis, the cathode was withdrawn, washed with deionized water thoroughly after the experiments of electrodepositing manganese. Subsequently, the passivation treatment with a 3% $K_2Cr_2O_7$ solution for 1.0 min was carried out, washed thoroughly with deionized water, and dried in an oven. The electrodeposits were weighed and scraped carefully from the cathode surface. Based on mass gained by the cathode, cathode current efficiency (η) was calculated by [19]

$$\eta = \frac{p}{E_{\mathrm{Mn}} J_{\mathrm{c}} A_{\mathrm{c}}}\left(\frac{\Delta m_{\mathrm{c}}}{\Delta t}\right)\times 100\% \quad (1)$$

where $\Delta m_c/\Delta t$ is the mass gain of the cathode over the time interval Δt (g/s); A_c is the effective cathode area (m^2); J_c is the applied current density (A/m^2); p is the purity of the electrodeposited manganese; E_{Mn} is the electrochemical equivalent of metallic manganese (1.025 g/(A·h)).

2.3 Characterization procedure

The manganese electrodeposits were analyzed by

SEM−EDS characterization using a Sirion 200 type SEM (FEI Company, Holland) aided to an EDS. To identify the structure of manganese electrodeposits, XRD tests were performed on a D/Max 2500 spectroscope (Rigaku Corporation, Japan) with graphite monochromatized Cu K_α radiation (λ=1.5418 Å, 40 kV) in the 2θ range of 10° to 80° at a scan rate of 8.0 (°)/min. X-ray photo-electron spectrometry analysis (XPS, ESCALAB250Xi, Thermo Scientific monochromated Al K_α source, 1486.7 eV, 2 μm diameter beam), was used to determine the surface elemental distributions of electrodeposits.

2.4 Cathode polarization test

The cathode polarization tests were carried out by using a CHI760E electrochemical workstation in a conventional three-electrode glass cell with 100 mL electrolyte at (30±1) °C. A stainless-steel (AISI 301) working electrode was coated with epoxy resin, leaving an area of 0.25 cm^2 for the cathode polarization test. The working electrode surface was finely polished with 1800, 2000 and 3500 grit metallographic sandpaper to a mirror finish and then rinsed with alcohol followed by deionized water. A platinum sheet (2.8 cm^2) was used as a counter electrode, and the reference electrode was a saturated calomel electrode (SCE). All potentials were recorded vs SCE through a Luggin capillary. The cathode potential was scanned in the potential range from −0.5 to −1.7 V at a rate of 1 mV/s. High purity nitrogen was used to sparge out the dissolved oxygen and maintain an inert atmosphere throughout the polarization test.

3 Results and discussion

3.1 Manganese electrodeposition analysis

3.1.1 Effect of Na_2SiO_3 concentration on cathode current efficiency

In order to investigate the effect of Na_2SiO_3 concentration on cathode current efficiency, the experiments of manganese electrodeposition were performed with Na_2SiO_3 concentrations varying from 0 to 5.7×10^{-3} mol/L under previous optimized conditions: 0.55 mol/L Mn^{2+}, 0.91 mol/L $(NH_4)_2SO_4$, 3.6×10^{-4} mol/L SeO_2, pH 7.0, stirring rate of 150 r/min, cathode current density of 400 A/m^2, electrodeposition temperature of 30 °C and time of 60 min. Figure 1 shows that cathode current efficiency increases significantly from 76.31% to 92.75% when Na_2SiO_3 concentration increases from 0 to 8.2×10^{-4} mol/L in the catholyte, and cathode current efficiency remains constant nearly when Na_2SiO_3 concentration increases from 8.2×10^{-4} to 1.6×10^{-3} mol/L. The current efficiency decreases slowly when Na_2SiO_3 concentration exceeds 1.6×10^{-3} mol/L. The cathode current efficiency is influenced by the competitive reactions, i.e., manganese deposition and hydrogen evolution reaction on the cathode surface simultaneously. Cathode current efficiency depends on the relative rate of manganese electrodeposition compared with that of hydrogen evolution reaction. Within the silicate solubility (0.2 mol/L, 25 °C), silicate exists in the form of monomeric silicate species. Therefore, after the addition of Na_2SiO_3 inhibitor, the hydrolysis of Na_2SiO_3 at lower concentrations (5.7×10^{-3} mol/L) may produce a number of monomeric silicate species, such as SiO_3^{2-} and $HSiO_3^-$ anions. These silicate anions may adsorb on the electrode surface to block the active sites for hydrogen evolution reaction and manganese electrodeposition [20,21]. On the other hand, the formation of hydrophilic complexes between Mn^{2+} and Si-containing anions results in the decrease of Mn^{2+} ion concentration, which leads to the increase of concentration polarization on the cathode surface. Two effects lead to the increase of the overpotential of hydrogen evolution reaction. Thus, hydrogen evolution reaction is significantly inhibited, which can indirectly increase the relative rate of manganese electrodeposition and then improve the cathode current efficiency. However, with the increase of Na_2SiO_3 concentration, the products of Na_2SiO_3 hydrolysis, i.e., monomeric polymeric and colloidal species, also hinder manganese electrodeposition due to the impoverishment of Mn^{2+} ions on the cathode surface, which indirectly results in the decrease of the cathode current efficiency.

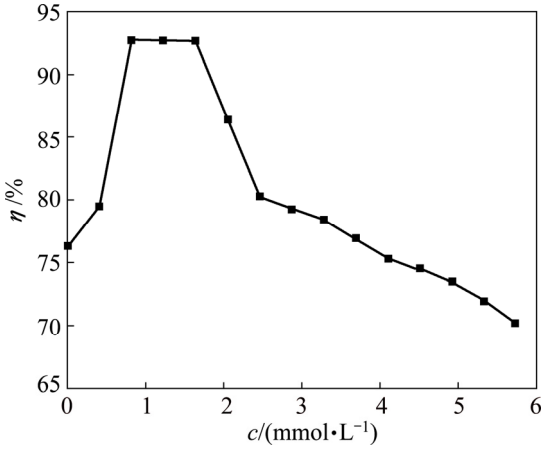

Fig. 1 Effect of Na_2SiO_3 concentration (c) on cathode current efficiency (η)

3.1.2 Effect of initial pH on cathode current efficiency

Manganese electrodeposition experiments were performed by varying the initial pH from 6.0 to 9.5 under previous conditions: 0.55 mol/L Mn^{2+}, 0.91 mol/L $(NH_4)_2SO_4$, 3.6×10^{-4} mol/L SeO_2, 8.2×10^{-4} mol/L Na_2SiO_3, 400 A/m^2, 150 r/min, 30 °C and 60 min. The results are plotted in Fig. 2. As indicated in Fig. 2, cathode current efficiency rises sharply from 71.9% at pH 6.0 to 81.87% at pH 7.0 and then stabilizes in the pH

region of 7.0−8.5; it decreases from 81.45% at pH 8.5 to 72.34% at pH 9.5. Hydrogen evolution reaction on the electrode surface is obvious and cathode current efficiency decreases when the initial pH is less than 7.0. With manganese electrodeposition proceeding, H^+ is depleted in the electrolyte near the cathode surface due to the hydrogen evolution reaction. Cathode current efficiency is influenced by the relative rate of manganese electrodeposition compared with that of hydrogen evolution reaction [22]. However, the rate of hydrogen evolution reaction declines as the pH increases continuously, which is conducive to manganese electrodeposition. Moreover, with continuous increase of the pH, a yellow precipitate of $Mn(OH)_2$ is formed when the initial pH is higher than 7.8 [19]. This will lead to the consumption of manganese ions and the increase of the electronic transfer resistance on the electrode surface, which may result in the decrease of the cathode current efficiency. Hence, optimal pH 7.0−8.0 is determined to obtain higher cathode current efficiency.

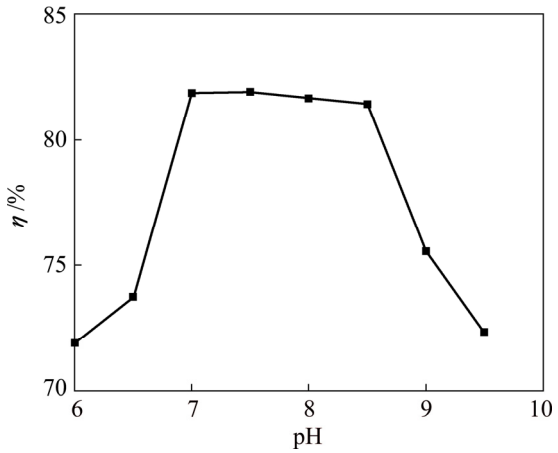

Fig. 2 Effect of initial pH on cathode current efficiency

3.2 Effect of Na_2SiO_3 concentration on structure of manganese electrodeposits

3.2.1 SEM−EDS analysis of manganese electrodeposits

To analyze the influence of Na_2SiO_3 concentration on the morphology of manganese electrodeposits, SEM tests were carried out. The morphology of manganese electrodeposits is shown in Fig. 3. The SEM observation of manganese electrodeposits without Na_2SiO_3 (Fig. 3(a)) shows a rough morphology and presents zones of imperfections with the presence of cracks and pores. It was reported that the presence of cracks and pores would deteriorate the properties of metal electrodeposits, especially the corrosion resistance [16]. Whereas, SEM image (Fig. 3(b)) presents a gray, shining and covering most of the surface after the presence of 8.2×10^{-4} mol/L Na_2SiO_3 in electrolyte. Figure 3(b) also shows that most of cracks and pores disappear on electrodeposit surface. Moreover, the presence of silicate anions in electrolyte forms a barrier against the gas diffusion and slows down the spread of vacuum pores and imperfections during the process of manganese electrodeposition [17].

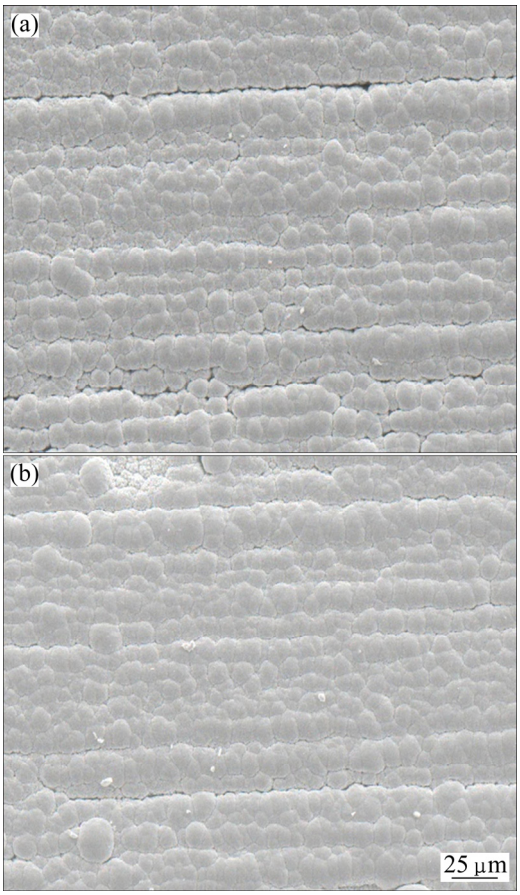

Fig. 3 SEM images of manganese electrodeposits at different Na_2SiO_3 concentrations: (a) 0; (b) 8.2×10^{-4} mol/L

Correspondingly, EDS analysis was carried out to investigate the chemical composition. The EDS patterns of the manganese electrodeposits before and after addition of Na_2SiO_3 are presented in Fig. 4. Electrodeposits obtained in absence of Na_2SiO_3 (Fig. 4(a)) were compared with those of Na_2SiO_3 addition into the electrolyte (Fig. 4(b)). Both electrodeposits contain 100% manganese nearly. Figure 4(b) indicates that silicon is absent in the manganese electrodeposit detected by EDS test although Na_2SiO_3 is added into the electrolyte.

3.2.2 XRD analysis of manganese electrodeposits

The crystal structures of manganese electrodeposits were studied by XRD. The results are shown in Fig. 5. Figure 5 shows the Bragg peaks of Fig. 5(a) are similar to those of Fig. 5(b). The addition of Na_2SiO_3 into electrolyte results in a slight shift to right of the biggest peak in Fig. 5(b), which results from the influence of silicate on electrodeposition process. A similar result has been observed during Ni electroplating process in silicate solution elsewhere [22]. Moreover, the Bragg peaks of

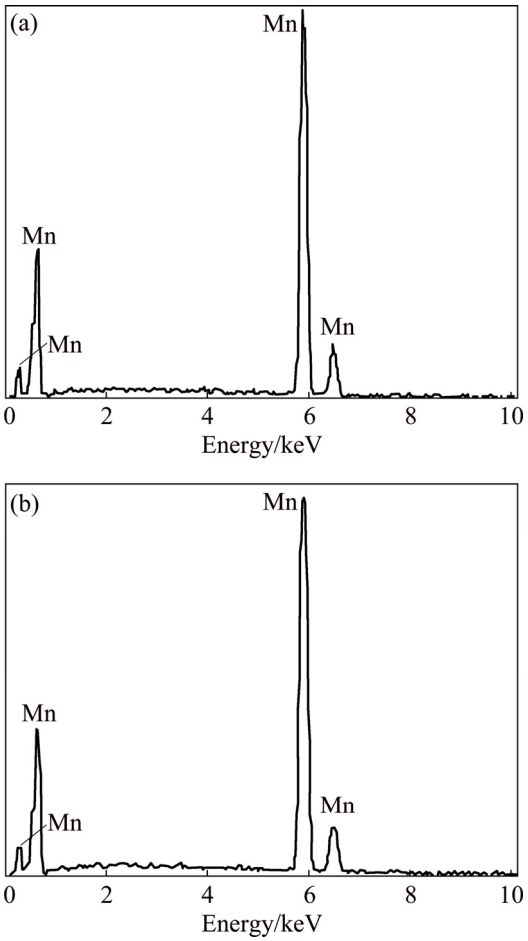

Fig. 4 EDS patterns of manganese electrodeposits at different Na_2SiO_3 concentrations: (a) 0; (b) 8.2×10^{-4} mol/L

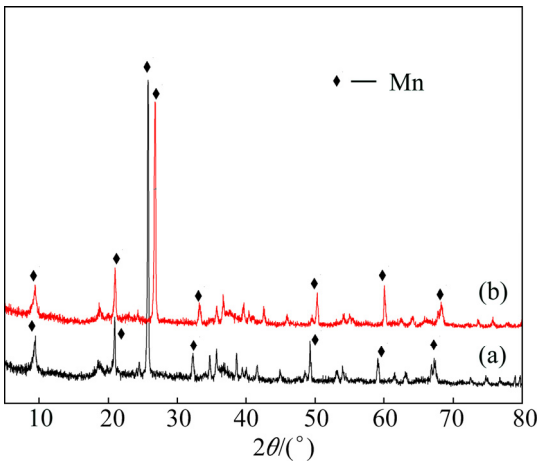

Fig. 5 XRD patterns of manganese electrodeposits at different Na_2SiO_3 concentrations: (a) 0; (b) 8.2×10^{-4} mol/L

Fig. 5(b) are slightly broader and less intensive compared with those of Fig. 5(a). This may be due to nano-crystalline or amorphous or their mixed structure. Furthermore, it was reported that the presence of well-defined cauliflowers structure characterized that silicate anions were adsorbed on metal surface [23−25]. This result was further confirmed by the morphology as shown in Fig. 3(b).

3.2.3 XPS analysis of manganese electrodeposits

To further analyze the chemical compositions of manganese electrodeposits, XPS measurement was performed. In this section, the chemical states of manganese, silicon and oxygen on the surface of manganese electrodeposits are focused. The XPS spectra of Mn 2p are limited values due to difficulty in differentiating among the contributions of different valences for most solid Mn phases [26]. Hence, Mn $2p_{3/2}$ XPS spectra are currently used to investigate the chemical state of Mn element. Figure 6 shows Mn 2p XPS spectra concerning double peaks Mn $2p_{3/2}$ and Mn $2p_{1/2}$ of manganese electrodeposits obtained at different Na_2SiO_3 concentrations in the catholyte. The Mn $2p_{3/2}$ peaks appear at about 641.71 eV for the manganese electrodeposits, which is in the range of 640.9−642.5 eV for Mn $2p_{3/2}$ standard peak position in the manganese oxide [27]. The peak position of Mn $2p_{3/2}$ spectra suggests that the manganese electrodeposits are slightly oxidized. Moreover, Mn $2p_{3/2}$ spectra peaks are asymmetry, which also indicates that manganese elements may be in the presence of more than one chemical state. It is concluded from Fig. 6 that manganese atoms on electrodeposit surface are probably oxidized.

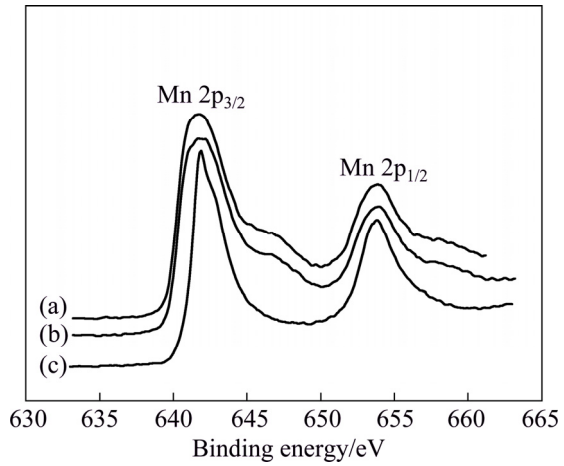

Fig. 6 XPS patterns of Mn 2p for manganese electrodeposits at different Na_2SiO_3 concentrations: (a) 8.2×10^{-4} mol/L; (b) 1.6×10^{-3} mol/L; (c) 2.5×10^{-3} mol/L

The surfaces of manganese electrodeposits with or without addition of Na_2SiO_3 were characterized using a variety of XPS peak positions. However, Si 2p binding energy is the key peak to pivot primarily on the results [28]. The Si 2p energy can give specific information of chemical environment to characterize the surface. Figure 7 presents the Si 2p binding energies of manganese electrodeposits at different Na_2SiO_3 concentrations in catholyte. Figure 7 shows the large peak in the range from 101.6 to 102.4 eV, indicating that

trace of silicate species have presumably been mixed into manganese electrodeposits surface [16,28].

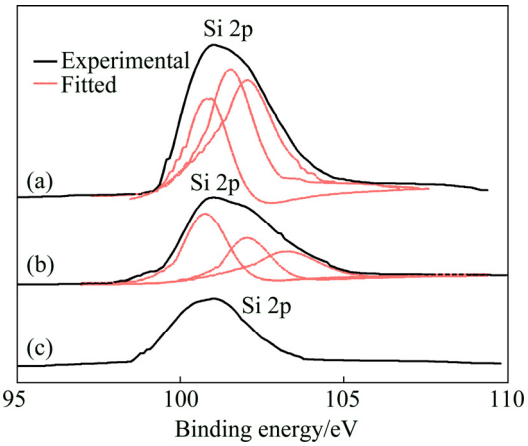

Fig. 7 Si 2p XPS patterns for manganese electrodeposits at different Na_2SiO_3 concentrations: (a) 8.2×10^{-4} mol/L; (b) 1.6×10^{-3} mol/L; (c) 2.5×10^{-3} mol/L

To further analyze the chemical state of oxygen atoms on the surface, XPS characterization was accordingly performed. The O 1s XPS patterns are often used to investigate chemical state of oxygen atom. Figure 8 shows O 1s XPS patterns for manganese electrodeposits of different concentration of Na_2SiO_3. The O 1s peaks appear in the range of 529.53−529.69 eV for manganese electrodeposits, which is in the range of 640.9−642.5 eV for O 1s standard peak position in metal oxide [26]. In addition, O 1s spectra peaks are also asymmetry, which also indicates that oxygen elements may be in the presence of more than one chemical state.

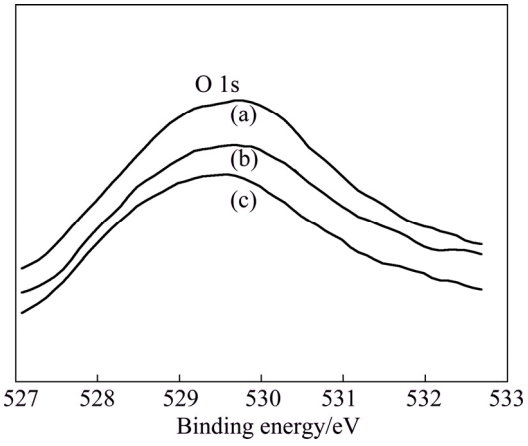

Fig. 8 O 1s XPS patterns for manganese electrodeposits at different Na_2SiO_3 concentrations: (a) 8.2×10^{-4} mol/L; (b) 1.6×10^{-3} mol/L; (c) 2.5×10^{-3} mol/L

3.3 Solution chemistry calculation

3.3.1 Solution chemistry calculation of sulfate electrolyte

In aqueous sulfate electrolyte solution (25 °C), the distributions of Mn species are influenced by several ions, including SO_4^{2-}, NH_4^+ and OH^-. Several chemical equilibria involving Mn^{2+} forms are present in aqueous sulfate electrolyte [29−31]. The equilibrium reactions are listed in Table 1.

According to equilibria and coefficients (Table 1), total concentration of Mn species ($[Mn]_T$) can be expressed as follows:

$$[Mn]_T=[Mn^{2+}]+[Mn(OH)^+]+[Mn(OH)_2(aq)]+[Mn(OH)_3^-]+[Mn(OH)_4^{2-}]+[MnSO_4]+[Mn(SO_4)_2^{2-}]+[MnHSO_4^-]+[Mn(NH_3)^{2+}]+[Mn(NH_3)_2^{2+}]+[Mn(NH_3)_3^{2+}]+[Mn(NH_3)_4^{2+}] \quad (18)$$

then

$$[Mn]_T=[Mn^{2+}](1+K_1[OH^-]+K_2[OH^-]^2+K_3[OH^-]^3+K_4[OH^-]^4+K_5[SO_4^{2-}]+K_6[SO_4^{2-}]^2+K_7K_8[H^+][SO_4^{2-}]+K_9K_{10}[OH^-][NH_4^+]+K_{11}K_9^2[OH^-]^2[NH_4^+]^2+K_{12}K_9^3[OH^-]^3[NH_4^+]^3+K_{13}K_9^4[OH^-]^4[NH_4^+]^4) \quad (19)$$

So, the concentration of different Mn^{2+} species is calculated by introducing a side reaction coefficient $\alpha_{Mn^{2+}}$:

$$\alpha_{Mn^{2+}}=\frac{[Mn]_T}{[Mn^{2+}]}=(1+K_1[OH^-]+K_2[OH^-]^2+K_3[OH^-]^3+K_4[OH^-]^4+K_5[SO_4^{2-}]+K_6[SO_4^{2-}]^2+K_7K_8[H^+][SO_4^{2-}]+K_9K_{10}[OH^-][NH_4^+]+K_{11}K_9^2[OH^-]^2[NH_4^+]^2+K_{12}K_9^3[OH^-]^3[NH_4^+]^3+K_{13}K_9^4[OH^-]^4[NH_4^+]^4) \quad (20)$$

Then, $[Mn^{2+}]$ of free Mn^{2+} is expressed by

$$[Mn^{2+}]=\frac{[Mn]_T}{\alpha_{(Mn^{2+})}} \quad (21)$$

Similarly, $[SO_4^{2-}]$ and $[NH_4^+]$ of free SO_4^{2-} and NH_4^+ ions are expressed by

$$[SO_4^{2-}]=\frac{[SO_4^{2-}]_T}{\alpha_{SO_4^{2-}}} \quad (22)$$

with

$$\alpha_{SO_4^{2-}}=1+K_5[Mn^{2+}]+2K_6[Mn^{2+}][SO_4^{2-}]+K_7[H^+]+K_7K_8[H^+][Mn^{2+}]+K_{14}[H^+]^2+K_7K_9K_{15}K_w[NH_4^+] \quad (23)$$

and

$$[NH_4^+]=\frac{[NH_4^+]_T}{\alpha_{NH_4^+}} \quad (24)$$

Table 1 Constants for equilibrium reactions of Mn species at 25 °C

Reaction	Equilibrium coefficient	Reaction No.	Constant
$Mn^{2+}+OH^- \rightleftharpoons Mn(OH)^+$	$K_1=\frac{[Mn(OH)^+]}{[Mn^{2+}][OH^-]}$	(2)	$K_1=10^{3.54}$
$Mn^{2+}+2OH^- \rightleftharpoons Mn(OH)_2(aq)$	$K_2=\frac{[Mn(OH)_2]}{[Mn^{2+}][OH_2]}$	(3)	$K_2=10^{5.8}$
$Mn^{2+}+3OH^- \rightleftharpoons Mn(OH)_3^-$	$K_3=\frac{[Mn(OH)_3^-]}{[Mn^{2+}][OH^-]^3}$	(4)	$K_3=10^{7.2}$
$Mn^{2+}+4OH^- \rightleftharpoons Mn(OH)_4^{2-}$	$K_4=\frac{[Mn(OH)_4^{2-}]}{[Mn^{2+}][OH^-]^4}$	(5)	$K_4=10^{7.3}$
$Mn^{2+}+SO_4^{2-} \rightleftharpoons MnSO_4$	$K_5=\frac{[MnSO_4]}{[Mn^{2+}][SO_4^{2-}]}$	(6)	$K_5=10^{2.25}$
$Mn^{2+}+2SO_4^{2-} \rightleftharpoons Mn(SO_4)_2^{2-}$	$K_6=\frac{[MnSO_4]}{[Mn^{2+}][SO_4^{2-}]^2}$	(7)	$K_6=10^{1.87}$
$H^++SO_4^{2-} \rightleftharpoons HSO_4^-$	$K_7=\frac{[HSO_4^-]}{[H^+][SO_4^{2-}]}$	(8)	$K_7=10^{0.52}$
$Mn^{2+}+HSO_4^- \rightleftharpoons MnHSO_4^+$	$K_8=\frac{[MnHSO_4^+]}{[Mn^{2+}][HSO_4^-]}$	(9)	$K_8=10^{2.26}$
$NH_4^++OH^- \rightleftharpoons NH_3\cdot H_2O$	$K_9=\frac{[NH_3\cdot H_2O]}{[NH_4^+][OH^-]}$	(10)	$K_9=10^{4.74}$
$Mn^{2+}+NH_3 \rightleftharpoons Mn(NH_3)^{2+}$	$K_{10}=\frac{[Mn(NH_3)^{2+}]}{[Mn^{2+}][NH_3]}$	(11)	$K_{10}=10^{0.908}$
$Mn^{2+}+2NH_3 \rightleftharpoons Mn(NH_3)_2^{2+}$	$K_{11}=\frac{[Mn(NH_3)_2^{2+}]}{[Mn^{2+}][NH_3]^2}$	(12)	$K_{11}=10^{1.38}$
$Mn^{2+}+3NH_3 \rightleftharpoons Mn(NH_3)_3^{2+}$	$K_{12}=\frac{[Mn(NH_3)_3^{2+}]}{[Mn^{2+}][NH_3]^3}$	(13)	$K_{12}=10^{1.58}$
$Mn^{2+}+4NH_3 \rightleftharpoons Mn(NH_3)_4^{2+}$	$K_{13}=\frac{[Mn(NH_3)_4^{2+}]}{[Mn^{2+}][NH_3]^4}$	(14)	$K_{13}=10^{1.53}$
$H^++HSO_4^- \rightleftharpoons H_2SO_4$	$K_{14}=\frac{[H_2SO_4]}{[H^+][HSO_4^-]}$	(15)	$K_{14}=10^{1.12}$
$NH_3+HSO_4^- \rightleftharpoons NH_4SO_4^-$	$K_{15}=\frac{[NH_4SO_4^-]}{[NH_3][HSO_4^-]}$	(16)	$K_{15}=10^{1.03}$
$H_2O \rightleftharpoons H^++HO^-$	$K_w=[H^+][OH^-]$	(17)	$K_w=10^{-14}$

with

$$\alpha_{NH_4^+}=1+K_9[OH^-]+K_9K_{10}[Mn^{2+}][OH^-]+2K_9^2K_{11}[Mn^{2+}][OH^-]^2[NH_4^+]+3K_9^3K_{12}[Mn^{2+}][OH^-]^3[NH_4^+]^2+4K_9^4K_{13}[Mn^{2+}][OH^-]^4[NH_4^+]^3+K_wK_7K_9K_{15}[SO_4^{2-}] \quad (25)$$

According to Eqs. (2)−(25) and constants, distributions of the main species in sulfate electrolyte are shown in Fig. 9. Figure 9(a) shows Mn species of sulfate electrolyte, in the pH range of 7.0−7.5, primarily are $MnSO_4$, $Mn(SO_4)_2^{2-}$, Mn^{2+} and $Mn(NH_3)^{2+}$. Moreover, other species of containing Mn^{2+} ions, such as $Mn(OH)_m^{2-m}$ (m=1−4) and $Mn(NH_3)_n^{2+}$ (n=1−4) are also present, but these species are only a small proportion of total Mn^{2+} concentration. Figure 9(b) presents that distributions of NH_4^+ and SO_4^{2-} are primary species of non-metallic ions in sulfate electrolyte.

3.3.2 Solution chemistry calculation of Na_2SiO_3

The hydrolysis is prone to occur in aqueous sodium silicate solution. So, there are little SiO_3^{2-} anions, but lots of $H_2SiO_4^{2-}$ and $H_3SiO_4^-$ are present in sodium silicate solution. Within its silicate solubility (0.2 mol/L, 25 °C), silicate exists in the form of monomeric silicate species. Polymerization of silicate occurs when the concentration surpasses its solubility in solution. The addition amount of Na_2SiO_3 is generally within its solubility when it is used in mineral processing as a flotation regulator. In this work, the ranges of 0−5.7×10^{-3} mol/L Na_2SiO_3 and pH 7.0−8.0 were applied for manganese electrodeposition

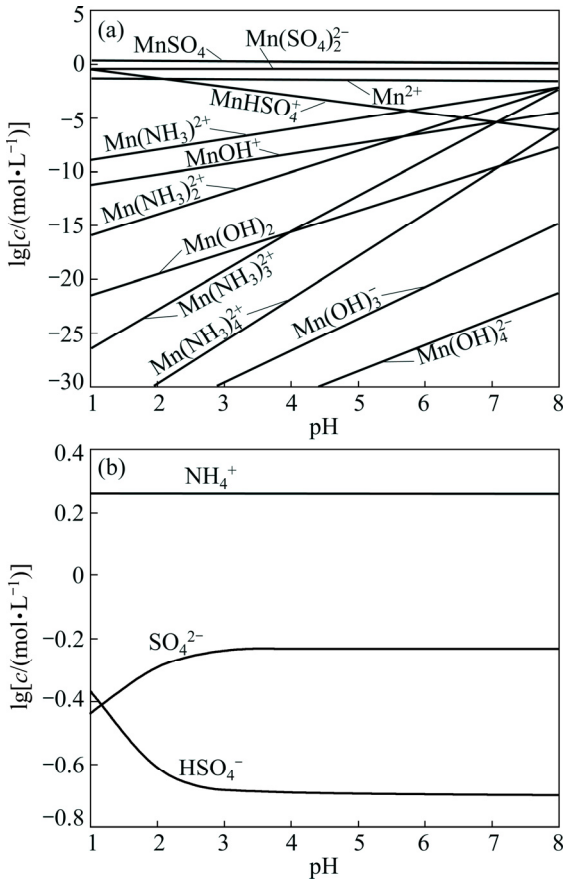

Fig. 9 Relationship between lg c and pH in sulfate electrolyte (0.55 mol/L $MnSO_4$, 0.91 mol/L $(NH_4)_2SO_4$): (a) Mn species; (b) Non-metallic species

process. Thus, if polymerization of silicic acid could not be taken into account, primary equilibrium relationship and corresponding constants are described in aqueous sodium silicate solution (25 °C) [29,32].

$$Na_2SiO_3+H_2O \rightleftharpoons NaHSiO_3+NaOH \quad (26)$$

$$H^+ + SiO_3^{2-} \rightleftharpoons HSiO_3^-,\ K_1^H = \frac{[HSiO_3^-]}{[H^+][SiO_3^{2-}]} = 1\times10^{13.1} \quad (27)$$

$$HSiO_3^- + H^+ \rightleftharpoons H_2SiO_3,\ K_2^H = \frac{[H_2SiO_3]}{[H^+][HSiO_3^-]} = 1\times10^{9.86} \quad (28)$$

where K_1^H and K_2^H represent the protonation constants of silicate anions. From Eqs. (26)−(28), silicate species are formed in electrolyte, including H_2SiO_3, $HSiO_3^-$ and SiO_3^{2-}. The initial total concentration of sodium silicate (c_T) can be evaluated through the following formula:

$$c_T = [HSiO_3^-] + [H_2SiO_3] + [SiO_3^{2-}] \quad (29)$$

According to Eqs. (26)−(28), the relative parameters are replaced into Eq. (29), Eqs. (30)−(32) can be deduced:

$$[SiO_3^{2-}] = \frac{c_T}{1+1\times10^{13.1}[H^+]+1\times10^{13.1+9.86}[H^+]^2} \quad (30)$$

$$[HSiO_3^-] = \frac{1\times10^{13.1}c_T[H^+]}{1+1\times10^{13.1}[H^+]+1\times10^{13.1+9.86}[H^+]^2} \quad (31)$$

$$[H_2SiO_3] = \frac{1\times10^{13.1+9.86}c_T[H^+]^2}{1+1\times10^{13.1}[H^+]+1\times10^{13.1+9.86}[H^+]^2} \quad (32)$$

Therefore, the relationships between distributions of silicate species with varying pH of different c_T were calculated by Eqs. (28)−(30). The distributions of silicate species for a c_T (8.2×10^{-4} mol/L) are shown in Fig. 10.

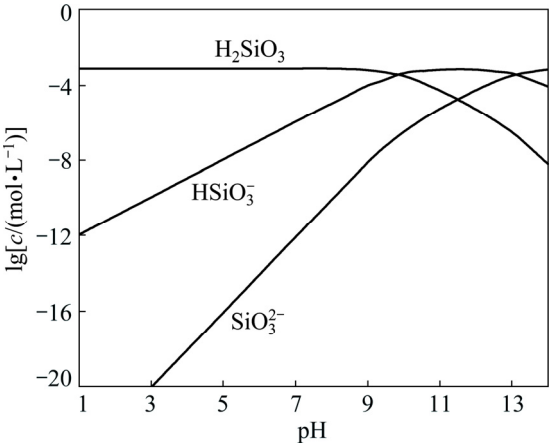

Fig. 10 Relationship between lg c of silicate species and pH of Na_2SiO_3 solution (c_T=8.2×10^{-4} mol/L)

Figure 10 indicates that there are three components in 8.2×10^{-4} mol/L Na_2SiO_3 solution, including H_2SiO_3(aq), $HSiO_3^-$ and SiO_3^{2-}. Figure 10 also shows that the concentrations of H_2SiO_3(aq) and $HSiO_3^-$ are higher compared with that of SiO_3^{2-} in aqueous Na_2SiO_3 solution when the pH 7.0−8.0 is suitable for manganese electrodeposition. Meanwhile, the concentrations of $HSiO_3^-$ and SiO_3^{2-} anions increase as pH increases, which may lead to the increase of the negative charge near the electrode surface in the catholyte. If the pH is above 7.8, the precipitation of $Mn(OH)_2$ may occur [19]. Therefore, there may be two competitive reactions of $Mn(OH)_2$ and $MnSiO_3$ formation on cathode surface simultaneously. Further, $MnSiO_3$ may inhibit the formation of $Mn(OH)_2$ on the cathode surface.

3.4 Thermodynamic analysis

Figure 10 shows that $MnSiO_3$ may form after the addition of Na_2SiO_3. Moreover, insoluble manganese (II) hydroxide is likely to form when pH of electrolyte is above 7.8 in the Mn−H_2O system [19,29]. Thus, the following reactions of Mn^{2+} ions may occur:

$$Mn^{2+} + SiO_3^{2-} \rightleftharpoons MnSiO_3,$$
$$K_{sp} = [Mn^{2+}][SiO_3^{2-}] = 1\times10^{-13.1} \quad (33)$$

$Mn^{2+}+2OH^- \rightleftharpoons Mn(OH)_2(s)$,

$$K_{sp}=[Mn^{2+}][OH^-]^2=1\times10^{-12.6} \quad (34)$$

Meanwhile, Fig. 10 also indicates that $HSiO_3^-$ anions are the primary species in aqueous Na_2SiO_3 solution as pH range is 7.0−8.0. The following reaction between $Mn(OH)_2(s)$ and $HSiO_3^-$ may be deduced from Eqs. (17), (27), (33) and (34).

$Mn(OH)_2(s)+HSiO_3^- \rightleftharpoons MnSiO_3(s)+H_2O+OH^-$,

$$K=1\times10^{1.5} \quad (35)$$

The chemical equilibrium constant of Eq. (35) is large enough. Thus, it is inferred that Eq. (35) is relatively prone to occur.

Further, in order to determine whether $MnSiO_3$ forms in aqueous sulfate electrolyte solution, the analysis of electronic structure was carried out. The electronic configuration of manganese atom is $1s^22s^22p^63s^23p^63d^54s^2$. The electronic configuration of Mn^{2+} cation is $1s^22s^22p^63s^23p^63d^54s^0$. Therefore, Mn^{2+} cation has empty 4s orbit, which has the tendency of coordination reaction of dsp^3 hybrid. So, Mn^{2+} cation can form complexes with oxygen anions, due to its unpaired electrons.

According to Eqs. (27) and (28), side reaction coefficient ($\alpha_{SiO_3^{2-}}$) of SiO_3^{2-} anions is expressed as

$$\alpha_{SiO_3^{2-}}=1+K_1^H[H^+]+K_1^HK_2^H[H^+]^2 \quad (36)$$

Thus, conditional solubility product K'_{sp} of manganese silicate is supposed as follows:

$$K'_{sp}=K_{sp}\alpha_{Mn^{2+}}\alpha_{SiO_3^{2-}} \quad (37)$$

In balanced system (25 °C), change in standard Gibbs free energy (ΔG^Θ) can be used to estimate whether a reaction between Mn^{2+} and SiO_3^{2-} ions could occur [33]. ΔG^Θ can be calculated by substituting K'_{sp} into formula (37).

$$\Delta G^\Theta=RT\ln K'_{sp}=RT\ln(K_{sp}\alpha_{Mn^{2+}}\alpha_{SiO_3^{2-}}) \quad (38)$$

where R is the mole gas constant (8.314 J/(mol·K)); T is absolute temperature (K). According to Eqs. (20), (33), (36) and (38), the relationship between the calculated ΔG^Θ of Mn^{2+} and SiO_3^{2-} ions and pH is presented in Fig. 11.

Figure 11 indicates that ΔG^Θ gradually decreases as pH increases from 1.0 to 9.0. In the range of pH 7.0−8.0, ΔG^Θ reaches a lower negative value. Therefore, coordination reaction between Mn^{2+} and SiO_3^{2-} ions can occur. Thus, the complexes between Mn^{2+} and SiO_3^{2-} ions can stabilize Mn^{2+} cations and remain the aquated form at suitably low concentration, facilitating the evenness of manganese electrodeposits, which indirectly facilitates manganese electrodeposition as shown in Fig. 1.

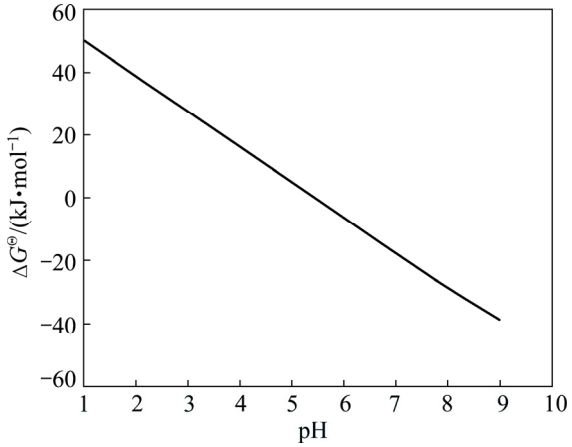

Fig. 11 Relationship between calculated ΔG^Θ of Mn^{2+} and SiO_3^{2-} ions and pH

3.5 Cathode polarization analysis

3.5.1 Cathode polarization analysis of Na_2SiO_3 on hydrogen evolution

Figure 12 shows the polarization curves with varying Na_2SiO_3 concentrations from 0 to 5.7×10^{-3} mol/L under the conditions: 0.91 mol/L $(NH_4)_2SO_4$, 3.6×10^{-4} mol/L SeO_2, pH 7.0 and 30 °C. The polarization curves shift sharply to negative direction as Na_2SiO_3 concentration in electrolyte increases. In the polarization test, it was observed that conspicuous hydrogen evolution started at about −1.0 V without Na_2SiO_3 in the electrolyte. However, inconspicuous hydrogen evolution started at about −1.2 V with 5.7×10^{-3} mol/L Na_2SiO_3 in the electrolyte. Figure 12 also presents that, at the same hydrogen evolution potential, the current density of Figs. 12(b) and (c) is lower than that of Fig. 12(a), which indicates that Na_2SiO_3 can improve the hydrogen evolution potential and then inhibit the hydrogen

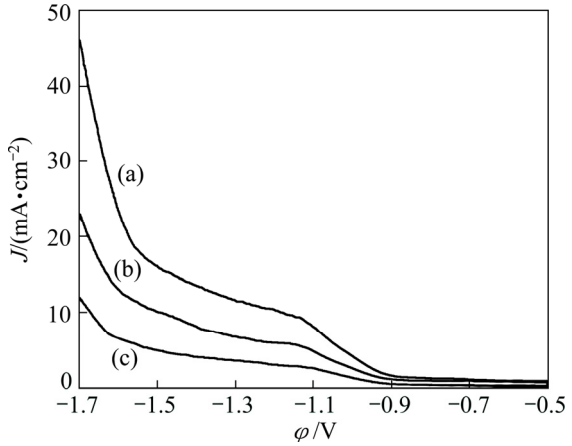

Fig. 12 Effect of Na_2SiO_3 concentration on cathode polarization curves of hydrogen evolution reaction under conditions of 0.91 mol/L $(NH_4)_2SO_4$, pH 7.0 and 30 °C at different Na_2SiO_3 concentrations: (a) 0; (b) 2.9×10^{-3} mol/L; (c) 5.7×10^{-3} mol/L

evolution on the cathode surface [34,35]. This can be probably attributed to the blocking of the active sites for hydrogen evolution reaction by the adsorption of the Si-containing ions on the electrode surface [20]. The inhibition effect of the hydrogen evolution is indirectly conducive to manganese electrodeposition as shown in Fig. 1.

3.5.2 Cathode polarization analysis of Na_2SiO_3 on manganese electrodeposition

To investigate influence of Na_2SiO_3 on manganese electrodeposition, cathode polarization tests were performed by changing Na_2SiO_3 concentration from 0 to 5.7×10^{-3} mol/L under the optimized conditions: 0.55 mol/L Mn^{2+}, 0.91 mol/L $(NH_4)_2SO_4$, 3.6×10^{-4} mol/L SeO_2, pH 7.0 and 30 °C. Figure 13 shows that the polarization curves shift to the negative direction evidently as Na_2SiO_3 concentration increases (Figs. 13(b) and (c)). That is, the deposition potentials decrease to more negative values with the increase of Na_2SiO_3 concentration. In cathode polarization tests, it is observed that, in the absence of Na_2SiO_3 (Fig. 13(a)), hydrogen evolution begins at around −1.1 V and the phenomenon of hydrogen evolution is obvious, and manganese electrodeposition is observed at about −1.3 V. However, in the presence of Na_2SiO_3 (Figs. 13(b) and (c)), hydrogen evolution reaction starts at about −1.2 V and the phenomenon of hydrogen evolution is inconspicuous, and manganese electrodeposition is observed at about −1.5 V. Hence, there are competitive reactions of hydrogen evolution reaction and manganese electrodeposition in the potential range of −1.2 to −1.5 V, and Na_2SiO_3 still has a significant inhibition effect on hydrogen evolution in the presence of Mn^{2+} ions. The process of manganese electrodeposition is observed in the potential range of −1.5 to −1.7 V. Moreover, the slope of Fig. 13(c) is slightly lower than that of Fig. 13(b) in the potential range of −1.5 to −1.7 V, which indicates that Na_2SiO_3 has a certain inhibition effect on manganese electrodeposition. This can be well responsible for the conclusions of Fig. 3. The inhibition effect of Na_2SiO_3 on manganese electrodeposition facilitates electro- depositing compact manganese metal. Moreover, it could be ascribed to the electrodeposition kinetic formula (Eq. (39)) [36].

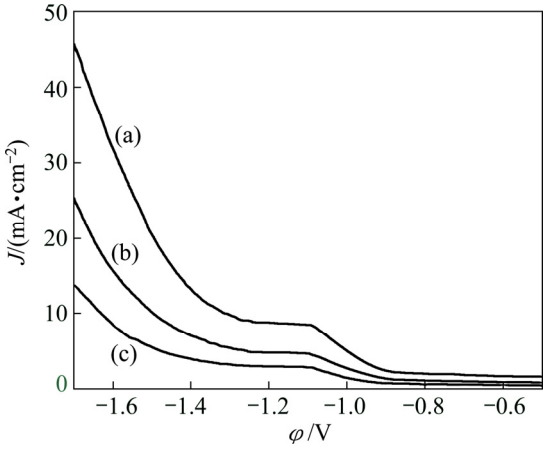

Fig. 13 Cathode polarization curves for manganese electrodeposition of manganese at different concentrations of Na_2SiO_3 (0.55 mol/L Mn^{2+}, 0.91 mol/L $(NH_4)_2SO_4$, 3.6×10^{-4} mol/L SeO_2, pH 7.0 and 30 °C) : (a) 0; (b) 2.9×10^{-3} mol/L; (c) 5.7×10^{-3} mol/L

$$R_1=A\exp(-B/\eta_1^2) \quad (39)$$

where R_1 is the number of nucleation; A and B are the overpotential-independent quantities; η_1 is the overpotential. That is, the increase of polarization promotes nucleation probability and hence improves structure of electrodeposits.

4 Conclusions

1) A certain amount of sodium silicate increases the cathode current efficiency of manganese electrodeposition. High current efficiency is obtained in the range of Na_2SiO_3 concentration from 8.2×10^{-4} to 1.6×10^{-3} mol/L and initial pH 7.0−8.0 under previous optimized condition.

2) SEM−EDS characterization demonstrates that sodium silicate can improve the imperfection surface of electrodeposited manganese. The nano-crystalline or amorphous structure is confirmed by XRD analysis. The chemical states of manganese, silicon and oxygen on the surface of manganese electrodeposits are determined by XPS analysis.

3) Solution chemistry calculations of manganese sulfate and sodium silicate indicate that Mn^{2+}, $MnSO_4$, $Mn(SO_4)_2^{2-}$, Mn^{2+}, $MnSiO_3$ and $Mn(NH_3)^{2+}$, SiO_3^{2-} and $HSiO_3^-$ are the main active ions during the process of manganese electrodeposition. The reaction between silicate and Mn^{2+} ions is confirmed by thermodynamic analysis.

4) The cathode polarization tests indicate that sodium silicate can increase the overpotential of hydrogen evolution and manganese electrodeposition. The overpotential increase of hydrogen evolution facilitates the improvement of the cathode current efficiency.

References

[1] TALIN A A, MARQUIS E A, GOODS S H, KELLY J J, MILLER M K. Thermal stability of Ni−Mn electrodeposits [J]. Acta Materialia, 2006, 54: 1935−1947.

[2] DÍAZ-ARISTA P, ORTIZ Z, RUIZ H, ORTEGA R, MEAS Y, TREJO G. Electrodeposition and characterization of Zn−Mn alloy coatings obtained from a chloride-based acidic bath containing ammonium thiocyanate as an additive [J]. Surface and Coatings Technology, 2009, 203: 1167−1175.

[3] GONG J, ZANGARI G. Electrodeposition of sacrificial tin/manganese alloy coatings [J]. Materials Science and Engineering A, 2003, 344: 268−278.

[4] QU De-yang. Investigation of the porosity of electrolytic manganese dioxide and its performance as alkaline cathode material [J]. Journal of Power Sources, 2006, 156: 692−699.

[5] PARK C H, JEON H S. The effect of sodium silicate as pH modifier and depressant in the froth flotation of molybdenite ores [J]. Materials Transactions, 2010, 51: 1367−1369.

[6] ARANTES R S, LIMA R M F. Influence of sodium silicate modulus on iron ore flotation with sodium oleate [J]. International Journal of Mineral Processing, 2013, 125: 157−160.

[7] MA M. The dispersive effect of sodium silicate on kaolinite particles in process water: Implication for iron-ore processing [J]. Clays & Clay Minerals, 2011, 59: 233−239.

[8] GONG W Q, KLAUBER C, WARREN L J. Mechanism of action of sodium silicate in the flotation of apatite from hematite [J]. International Journal of Mineral Processing, 1993, 39: 251−273.

[9] PARRENT M D. Separation of pyrolusite and hematite by froth flotation [D]. Edmonton: University of Alberta, 2012: 67−88.

[10] ANDRADE E M, COSTA B L C M, ALCÂNTARA G A G, LIMA R M F. Flotation of manganese minerals and quartz by sodium oleate and water glass [J]. Latin American Applied Research, 2012, 42: 39−43.

[11] STERTEN Å, SOLLI P A, SKYBAKMOEN E. Influence of electrolyte impurities on current efficiency in aluminium electrolysis cells [J]. Journal of Applied Electrochemistry, 1998, 28: 781−789.

[12] PADHY S K, PATNAIK P, TRIPATHY B C, BHATTACHARYA I N. Microstructural aspects of manganese metal during its electrodeposition from sulphate solutions in the presence of quaternary amines [J]. Materials Science and Engineering B, 2015, 193: 83−90.

[13] MURESAN L, MAURIN G, ONICIU L, GAGA D. Influence of metallic impurities on zinc electrowinning from sulphate electrolyte [J]. Hydrometallurgy, 1996, 43: 345−354.

[14] XU Fu-yuan, DAN Zhi-gang, ZHAO Wei-nan, HAN Gui-mei, SUN Ze-hui, XIAO Ke, JIANG Lin-hua, DUAN Ning. Electrochemical analysis of manganese electrodeposition and hydrogen evolution from pure aqueous sulfate electrolytes with addition of SeO_2 [J]. Journal of Electroanalytical Chemistry, 2015, 741: 149−156.

[15] DING Li-feng, FAN Xing, DU Jun, LIU Zuo-hua, TAO Chang-yuan. Influence of three N-based auxiliary additives during the electrodeposition of manganese [J]. International Journal of Mineral Processing, 2014, 130: 34−41.

[16] KUMARAGURU S P, VEERARAGHAVAN B, POPOV B N. Development of an electroless method to deposit corrosion-resistant silicate layers on metallic substrates [J]. Journal of the Electrochemical Society, 2006, 153: 253−259.

[17] SASSI W, DHOUIBI L, BERCOT P, REZRAZI M, TRIKI E. Study of the electroplating mechanism and physicochemical proprieties of deposited Ni−W-Silicate composite alloy [J]. Electrochimica Acta, 2014, 117: 443−452.

[18] MORKS M F, FAHIM N F, FRANCIS A A, SHOEIB M A. Fabrication and characterization of electro-codeposited Ni/Zr-silicate composite coating [J]. Surface and Coatings Technology, 2006, 201: 282−286.

[19] WEI Qi-feng, REN Xiu-lian, DU Jie, WEI Si-jie, HU Su-rong. Study of the electrodeposition conditions of metallic manganese in an electrolytic membrane reactor [J]. Minerals Engineering, 2010, 23: 578−586.

[20] CHANG Yu-chi. A kinetic model for the anodic dissolution of zinc in alkaline electrolyte with sodium metasilicate additions [J]. Electrochimica Acta, 1996, 41: 2425−2432.

[21] PATNAIK P, PADHY S K, TRIPATHY B C, BHATTACHARYA I N, PARAMGURU R K. Electrodeposition of cobalt from aqueous sulphate solutions in the presence of tetra ethyl ammonium bromide [J]. Transactions of Nonferrous Metals Society of China, 2015, 25(6): 2047−2053.

[22] REN Xiu-lian, WEI Qi-feng, LIU Zhe, LIU Jun. Electrodeposition conditions of metallic nickel in electrolytic membrane reactor [J]. Transactions of Nonferrous Metals Society of China, 2012, 22(2): 467−475.

[23] MONTEMOR M F, ROSQVIST A, FAGERHOLM H, FERREIRA M G S. The early corrosion behavior of hot dip galvanished steel pretreated with bis-1,2-(triethoxysily) ethane [J]. Progress in Organic Coatings, 2004, 51: 188−194.

[24] LEE J, KIM Y, CHUNG W. Effect of Ar bubbling during plasma electrolytic oxidation of AZ31B magnesium alloy in silicate electrolyte [J]. Applied Surface Science, 2012, 259: 454−459.

[25] AHMADI M, GUINEL M J F. Synthesis, characterization and understanding of the mechanisms of electroplating of nanocrystalline-amorphous nickel-tungsten alloys using in situ electrochemical impedance spectroscopy [J]. Journal of Alloys and Compounds, 2013, 574: 196−205.

[26] NESBITT H W, BANERJEE D. Interpretation of XPS Mn(2p) spectra of Mn oxyhydroxides and constraints on the mechanism of MnO_2 precipitation [J]. American Mineralogist, 1998, 83: 305−315.

[27] LÓPEZ-NAVARRETE E, CABALLERO A, GONZÁLEZ-ELIPE A R, OCAÑA M. Chemical state and distribution of Mn ions in Mn-doped α-Al_2O_3 solid solutions prepared in the absence and the presence of fluxes [J]. Journal of European ceramic society, 2004, 24: 3057−3062.

[28] HAHN J J, MCGOWAN N G, HEIMANN R L, BARR T L. Modification and characterization of mineralization surface for corrosion protection [J]. Surface and Coatings Technology, 1998, 108: 403−407.

[29] WANG Dian-zuo, HU Yue-hua. Solution chemistry of flotation [M]. Changsha: Hunan Science and Technology Press, 1988. (in Chinese)

[30] RUDNIK E. Effect of gluconate ions on electroreduction phenomena during manganese deposition on glassy carbon in acidic chloride and sulfate solutions [J]. The Journal of Electroanalytical Chemistry, 2015, 741: 20−31.

[31] TUNÇ M, YAPICI S, KOCAKERIM M M, YARTASI A. The dissolution kinetics of ulexite in sulphuric acid solutions [J]. Chemical and Biochemical Engineering Quarterly, 2001, 15: 175−180.

[32] PARK H, ENGLEZOS P. Osmotic coefficient data for Na_2SiO_3 and Na_2SiO_3−NaOH by an isopiestic method and modeling using Pitzer's model [J]. Fluid Phase Equilibria, 1998, 153: 87−104.

[33] QING Wen-qing, ZOU Song, LIU San-jun, LUO Hong-lin, LIU Rui-zeng, WANG Xing-jie. Solution chemistry mechanism of flotation of sodium oleate on rhodochrosite [J]. Journal of Wuhan University of Technology, 2014, 36: 124−129. (in Chinese)

[34] LU Jing, YANG Qi-hua, ZHANG Zhao. Effects of additives on nickel electrowinning from sulfate system [J]. Transactions of Nonferrous Metals Society of China, 2010, 20(1): 97−101.

[35] LUPI C, PASQUALI M, DELL'ERA A. Studies concerning nickel electrowinning from acidic and alkaline electrolytes [J]. Minerals Engineering, 2006, 19: 1246−1250.

[36] BICELLI L P, BOZZINI B, MELE C, D'URZO L. A Review of nanostructural aspects of metal electrodeposition [J]. International Journal of Electrochemical Science, 2008, 3: 356−408.

硅酸钠对硫酸盐溶液中电沉积锰的影响

薛建荣[1,2]，钟 宏[1]，王 帅[1]，李昌新[1]，武芳芳[1]

1. 中南大学 化学与化工学院，长沙 410083；
2. 湖南科技大学 化学与化工学院，湘潭 411201

摘 要：研究硅酸钠对硫酸盐溶液中锰电沉积的影响。锰电沉积实验结果表明，添加一定量的硅酸钠可以提高锰电沉积的阴极电流效率，且初始 pH 7.0~8.0 是获得较高阴极电流效率的 pH 优化值。扫描电子显微镜(SEM)和 X 射线衍射(XRD)分析结果表明，所得电沉积层呈致密、纳米晶结构。X 射线光电子能谱(XPS)分析结果表明，电沉积层中含 Mn、Si 和 O 元素。硫酸盐溶液和硅酸钠溶液化学计算结果表明，在锰电沉积过程中，Mn^{2+}、$MnSO_4$、$Mn(SO_4)_2^{2-}$、Mn^{2+}、$MnSiO_3$、$Mn(NH_3)^{2+}$、SiO_3^{2-}和 $HSiO_3^-$是主要的活性组分。Mn^{2+}与含硅离子的反应趋势经热力学计算分析证实。此外，极化曲线测试结果表明，添加硅酸钠可以提高析氢过电位，从而间接提高了阴极电流效率。

关键词：电沉积；锰；硅酸钠；电沉积层结构；析氢反应

(Edited by Wei-ping CHEN)